

• Supplementary File •

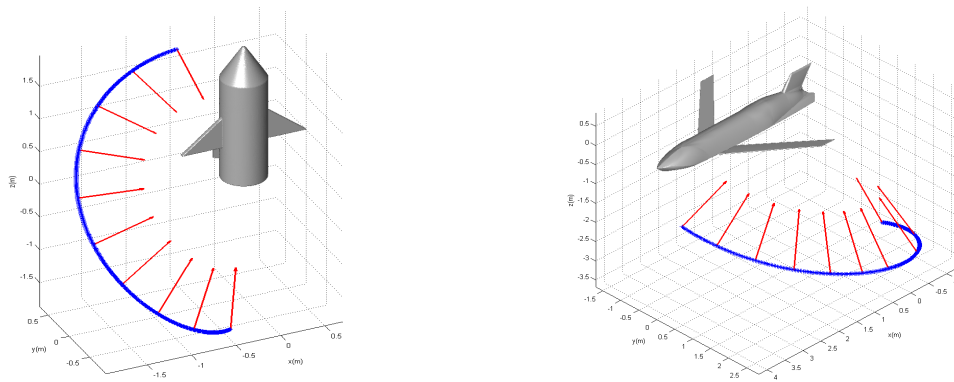
# Estimation of Vector Miss Distance for Complex Objects Based on Scattering Center Model

Jie WU<sup>1</sup>, Kunyi GUO<sup>1\*</sup>, Biyi WU<sup>1</sup> & Xinqing SHENG<sup>1</sup>

<sup>1</sup>*Institute of Applied Electromagnetic, School of Information and Electronics, Beijing Institute of Technology, Beijing 100081, China*

## Appendix A

The two objects are denoted by Object-1 and Object-2, as shown in Figure A1. Object-1 is a smaller aircraft with wing span width of 1 m and the fuselage length of 2 m. It has two side wings constructed by triangular plates, the fuselage constructed by a cone and a cylinder, and the tail constructed by parallelogram plates. Object-2 is a more complex object with wing span width of 3.4 m and fuselage length of 4.3 m, and it is constructed by irregular planes and curved surfaces. During the process of flying, the variation of the line of sight (LOS) in the body-fixed coordinate system is presented by blue lines in Figure A1.

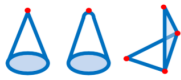

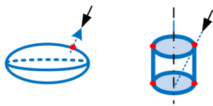


**Figure A1** The geometry of two objects (left: Object-1, right: Object-2)

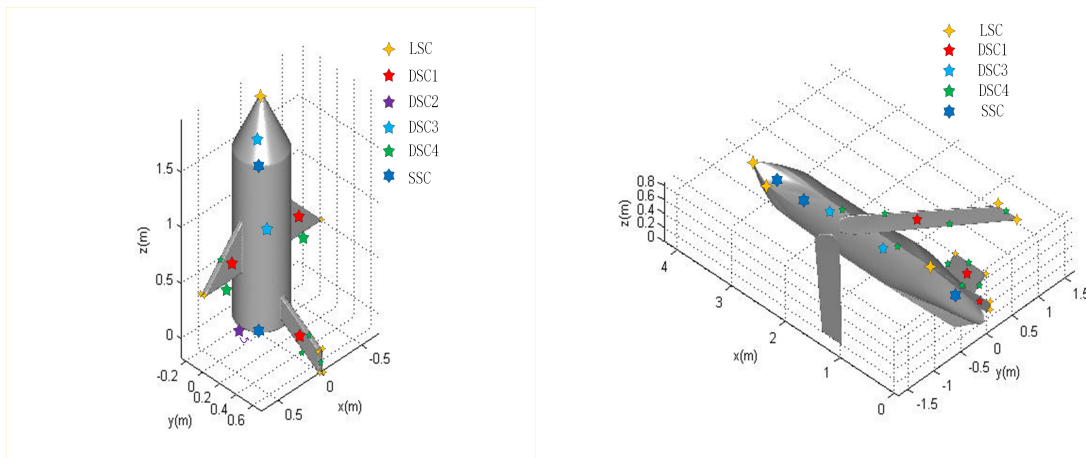
Based on the geometric structure and the formation mechanism of different types of scattering centers (SC) and the locations of SCs can be predicted [1,2], as shown in Figure A2, where LSC is localized SC, DSC is distributed SC and SSC is sliding SC. The SCs and their locations on the two objects are shown in Figure A3.

---

\* Corresponding author (email: guokunyi@bit.edu.cn)

	Locations	Examples
LSC	Sharp apex, conical cusp, small spherical top	
DSC	The center of straight-edge, plane; The center of generatrix (the intersection of the single-curved surface and the plane formed by the incident direction and rotation axis)	
SSC	The point on the double-curved surface where the normal direction is parallel to the incident direction; The intersection of the curved edge and the plane formed by incident direction and rotation axis.	

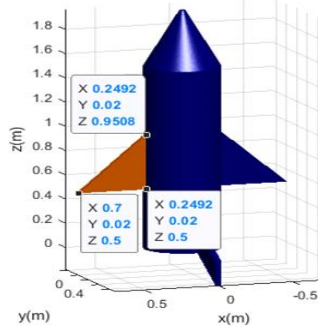
**Figure A2** Locations of scattering centers



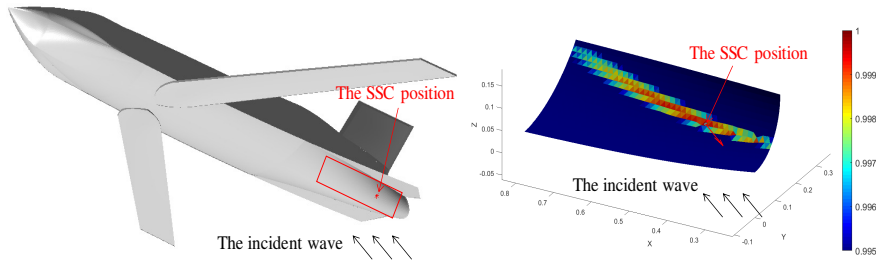
**Figure A3** Scattering centers of two objects (left: Object-1 right: Object-2)

The geometrical parameters of SCs can be extracted from the meshed CAD model of the objects. For the planar surface or straight edge, taking the DSC on the left side wing as an instance, we can read the coordinates of the vertices of the polygon, as illustrated in Figure A4.

For the curved surface, the effective back-reflected region can be obtained according to the normal directions of the mesh elements of the surface. Taking the SSC on the Object-2 as an instance, the effective back-reflected region is illustrated in Figure A5. To search the effective back-reflected region, we calculate the dot product of the normal direction of a facet and the direction of LOS:  $h = \hat{\mathbf{n}} \cdot \hat{\mathbf{r}}_{los}$ , where the direction of LOS is from the target to the radar. For the facet that has the maximum of  $h$ , we consider this facet is the effective back-reflected region. The location of the SSC is set as the geometrical center of this region. The location of SSC changes with the aspect angle of the LOS, therefore we need repeat the above process to acquire the changed location. It is worth mentioning that the precision of the extracted location is related to the size of mesh element. In this paper, the average length of the edges of triangular facets is set as one-tenth of the wavelength.



**Figure A4** The geometric parameter of DSC on the left side wing



**Figure A5** Extracting the SSC location from the meshed CAD model ( Left: The SSC position on the Object-2 when  $\theta = 137.2^\circ$ ,  $\phi = 96.9^\circ$ ; Right: The distribution of dot-product value in the region marked by the red square)

## Appendix B

The SC models for Object-1 and Object-2 are presented in Table B1 and B2. The simulation parameters are set as follows: for Object-1, the frequency of the incident wave is 3 GHz, the range of the aspect angle of the LOS is:  $\theta = 20^\circ \sim 159.8^\circ$  with a step of  $0.3^\circ$  and  $\phi = 150^\circ \sim 234^\circ$  with a step of  $0.18^\circ$ . For Object-2, the frequency of incident wave is 5 GHz, the aspect angle range of the LOS:  $\theta = 111^\circ \sim 157.2^\circ$  stepped by  $0.03^\circ$ , and  $\phi = 3^\circ \sim 157^\circ$  stepped by  $0.1^\circ$ . The polarization of the incident waves for both objects is VV.

**Table B1** Parametric models for Object-1

SCs of Object-1	Model	Parameters to be estimated
DSC1	$E^s = A_i \frac{4\hat{\mathbf{s}} \cdot \hat{\mathbf{n}}}{ \mathbf{w} ^2} \sum_{n=1}^N \mathbf{w}^* \cdot \mathbf{b}_n \text{sinc}(k\mathbf{w}^* \cdot \mathbf{b}_n) \exp[jk\mathbf{r}_c \cdot \mathbf{c}_n]$	$A_i (i = 1 \dots 8)$
DSC2	$E^s = A_i \frac{J_1(2ka \hat{\mathbf{s}} \times \hat{\mathbf{n}} )}{ \hat{\mathbf{s}} \times \hat{\mathbf{n}} } \exp(2jk\mathbf{r}_c \cdot \hat{\mathbf{s}})$	$A_i (i = 1)$
DSC3	$E^s = A_i W_c^i(\xi) \text{sinc}(kL\hat{\mathbf{s}} \cdot \hat{\boldsymbol{\tau}}) \exp(2jk\mathbf{r}_c \cdot \hat{\mathbf{s}})$	$A_i (i = 1, 2)$
DSC4	$E^s = A_i W_c^i(\xi) \text{sinc}(kL\hat{\mathbf{s}} \cdot \hat{\boldsymbol{\tau}}) \exp(2jk\mathbf{r}_c \cdot \hat{\mathbf{s}})$	$A_i (i = 1 \dots 7)$
LSC	$E^s = W_P(\xi, p_j, q_j) \exp(2jk\mathbf{r} \cdot \hat{\mathbf{s}})$	$A_i (i = 1 \dots 9), p_{ij}, q_{ij} (j = 1 \dots 5)$
SSC	$E^s(f, \xi) = A_i W_D(\xi) \exp(2jk\mathbf{r}_{ce}(\xi) \cdot \hat{\mathbf{s}})$	$A_i (i = 1, 2)$

In Table B1 (and the following Table B2),  $W_*(\xi)$  is related to the geometrical shape.

For conical surface,  $W_c(\xi) = \sqrt{L_c} \sin \gamma |\hat{\mathbf{s}} \times \hat{\mathbf{n}}|$ ,  $L_c$  is the length of the generatrix,  $\gamma$  is half conical angle of the cone.

For cylindrical surface,  $W_c(\xi) = \sqrt{a} |\hat{\mathbf{s}} \times \hat{\mathbf{n}}|$ , where  $a$  is the radius of the cylinder.

For DSC induced by the diffraction from a straight-edge with limited length:

$$W_e(\xi) = \frac{\sin \frac{\alpha}{2} [\sqrt{1-\mu} - \sqrt{2} \cos \frac{\alpha}{2}]}{\sin^2 \beta (\cos \alpha - \cot^2 \beta)} |\hat{\mathbf{s}} \times (\hat{\mathbf{s}} \times \hat{\mathbf{t}})| \quad (\text{B1})$$

where  $\mu = \cos \alpha - 2\cot^2 \beta$ ,  $\beta = \arccos(\hat{\mathbf{t}} \cdot \hat{\mathbf{s}})$ ,  $\hat{\alpha} = \frac{\hat{\mathbf{t}} \times \hat{\mathbf{s}}}{|\hat{\mathbf{t}} \times \hat{\mathbf{s}}|}$ ,  $\cos \alpha = \hat{\mathbf{n}} \cdot \hat{\alpha}$ ,  $\sin \alpha = \hat{\mathbf{t}} \cdot (\hat{\mathbf{n}} \times \hat{\alpha})$ ,  $\hat{\mathbf{t}}$  is the tangential direction of the straight edge,  $\hat{\mathbf{n}}$  is the normal direction of the plane on which the straight edge is located.  $\mathbf{r}_c$  is the position vector of the center of the straight edge.

For SSC induced by the diffraction from a curved edge:

$$W_D(\xi) = \frac{\sin \frac{\pi}{n}}{n\sqrt{\sin \xi}} [(\cos \frac{\pi}{n} - 1)^{-1} \mp (\cos \frac{\pi}{n} - \cos \frac{\pi + 2\xi}{n})^{-1}] \quad (\text{B2})$$

where  $n = 2 - \frac{\alpha}{\pi}$ ,  $\alpha$  is the splitting angle. For the SSC of Object-1 on the junction of the cone and the cylinder,  $\alpha = 153.2^\circ$ ; For the SSC of Object-1 on the bottom edge of the cylinder,  $\alpha = 90^\circ$ .  $\mathbf{r}_{ce}$  is the location vector of the point at which the edge intersects the incident plane in the illuminated area. The upper sign of  $\mp$  is for vertical polarization, and the lower sign is for horizontal polarization.

For LSC induced by the diffraction from geometric discontinuities:

$$W_P(\xi) = \frac{\sum_{i=1}^{N+1} p_i \xi^{i-1}}{\xi^N + \sum_{i=1}^N q_i \xi^{i-1}} \quad (\text{B3})$$

where  $p_i$  and  $q_i$  are coefficients of the rational polynomial, which are unknowns parameters to be estimated.  $N = 5$  in this paper.

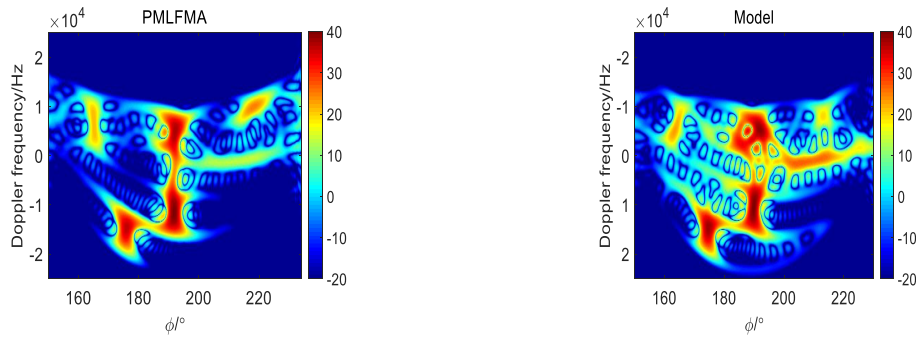
**Table B2** Parametric models for Object-2

SCs of Object-2	Model	Parameters to be estimated
DSC1	$E^s = A_i \frac{4\hat{s} \cdot \hat{n}}{ \mathbf{w} ^2} \sum_{n=1}^N \mathbf{w}^* \cdot \mathbf{b}_n \text{sinc}(k\mathbf{w}^* \cdot \mathbf{b}_n) \exp[jk\mathbf{w} \cdot \mathbf{c}_n]$	$A_i (i = 1, 2, 3)$
DSC3	$E^s = A_i W_c^i(\xi) \text{sinc}(kL\hat{s} \cdot \hat{\tau}) \exp(2jk\mathbf{r}_c \cdot \hat{s})$	$A_i (i = 1, 2)$
DSC4	$E^s = A_i W_c^i(\xi) \text{sinc}(kL\hat{s} \cdot \hat{\tau}) \exp(2jk\mathbf{r}_c \cdot \hat{s})$	$A_i (i = 1, 2, \dots, 9)$
LSC	$E^s = W_P(\xi, p_j, q_j) \exp(2jk\mathbf{r} \cdot \hat{s})$	$A_i (i = 1 \dots 9), p_{ij}, q_{ij} (j = 1 \dots 5)$
SSC	$E^s = W_P(\xi, p_j, q_j) \exp(2jk\mathbf{r} \cdot \hat{s})$	$A_i (i = 1, 2, 3), p_{ij}, q_{ij} (j = 1 \dots 5)$

In order to estimate the undetermined parameters of the SC models, the scattering fields from multiple aspect angles are computed by the full-wave method, MoM+PMLFMA [3]. Then from the scattering fields, the parameters of the models are estimated by genetic algorithm (GA). In GA, the maximum similarity of two time-frequency representation (TFR) images is chosen as the objective function (denoted as  $OF$ ).  $OF = 1 - \text{corrcoef}(TFR_o, TFR_e)$ , where  $TFR_o$  is the TFR of scattering fields computed by the full-wave method, and  $TFR_e$  is the TFR of scattering fields simulated by the SC model, and  $\text{corrcoef}(\cdot)$  means the correlation coefficient of the two TFRs.

In this letter, the TFR is used in the parameter estimation for two reasons. Firstly, TFR can separate the information of multiple SCs in the region of time-frequency, which is beneficial to the parameter estimation of multiple SCs; Secondly, the method of the vector miss distance (VMD) estimation adopted in this paper is based on Doppler frequency information. Therefore the simulation results by the SC models should have high similarity of Doppler characteristics. The joint time-frequency transform method adopted in this paper is the modified smoothing pseudo-Wigner-Ville transform algorithm (RSPWVD) [4], which has been proved to have high localization precision of Doppler frequencies and low level of cross-terms.

Using the above method, the parameters of the SC models of Object-1 and Object-2 are estimated. The TFR results simulated by the SC models and these computed by the full-wave method are shown in Figure B1 and Figure B2, respectively. The correlation coefficient of the TFRs in Figure B1 is 0.948 and that in Figure B2 is 0.858 respectively. Although the scattering fields computed by the full-wave numerical method are under uniform aspect angle sampling, it is possible to simulate the radar echoes of the objects under non-uniform sampling by using the SC models with the estimated parameters.

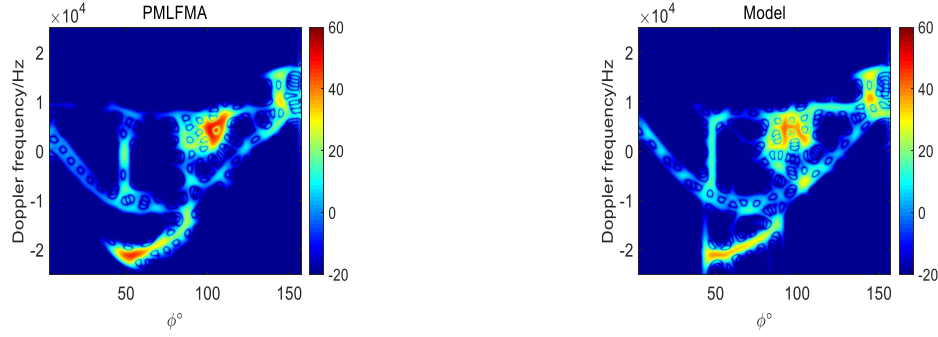


**Figure B1** TFRs of Object-1 (left: PMLFMA, right: SC model)

## Appendix C

### Appendix C.1 Object-1

There are significant DSCs on the flanks and the tails of Object-1, which is conducive to the estimation of VMD. The positions of the three receiving antennae are shown in Table Appendix C.1. The motion parameters of Object-1 are shown in Table Appendix C.1. Based on the given motion parameters, the range of the elevation angle ( $\theta$ ) is about  $20^\circ \sim 150^\circ$  and



**Figure B2** TFRs of Object-2 (left: PMLFMA right: SC model)

that of the azimuth angle ( $\phi$ ) is about  $150^\circ \sim 230^\circ$  for the short time interval (about 0.02 s) when the object is approaching to the CPA.

**Table C1** Antenna array coordinates

Number	$X_i$ (m)	$Y_i$ (m)	$Z_i$ (m)
1	0.8270	0	1.1696
2	0.8270	1.1696	0
3	0.8270	-1.1696	0

**Table C2** Simulation parameters

Parameters (unit)	Value	Parameters (unit)	Value
$X_{cpa}$ (m)	2.5162	$\alpha_v$ ( $^\circ$ )	-16.9
$Y_{cpa}$ (m)	1.8948	$\beta_v$ ( $^\circ$ )	28.1
$Z_{cpa}$ (m)	-0.9913	$\alpha_r$ ( $^\circ$ )	-28.7
$r$ (m)	3.3	$\beta_r$ ( $^\circ$ )	31.6
$v$ (m/s)	600	$a$ (m/s $^2$ )	0

**Table C3** Comparison of estimation results between the case of single antenna and that of three antennas

Parameters (unit)	Three Antennas	Absolute Error	Single Antenna	Absolute Error
$X_{cpa}$ (m)	2.5187	0.0025	2.8177	0.3015
$Y_{cpa}$ (m)	1.738	0.1568	2.0435	0.1487
$Z_{cpa}$ (m)	-1.0936	0.0723	-0.6702	0.3211
$r$ (m)	3.2397	0.0603	3.038	0.262
$v$ (m/s)	599.73	0.27	607.852	7.852
$\alpha_v$ ( $^\circ$ )	-15.906	0.794	-20.632	3.732
$\beta_v$ ( $^\circ$ )	28.762	0.662	23.977	4.123
$\alpha_r$ ( $^\circ$ )	-28.694	0.11	-30.6134	1.9134
$\beta_r$ ( $^\circ$ )	30.11	1.49	21.925	9.675

The VMD parameter is then set as the unknown parameters to be estimated. The comparison of estimation results of single antenna and those of three antennas for Object-1 are presented in Table C3 (where noise is not considered), which demonstrates that increasing the amounts of the antennas can improve the accuracy of the parameter estimation. The case of three antennas are only considered in the following.

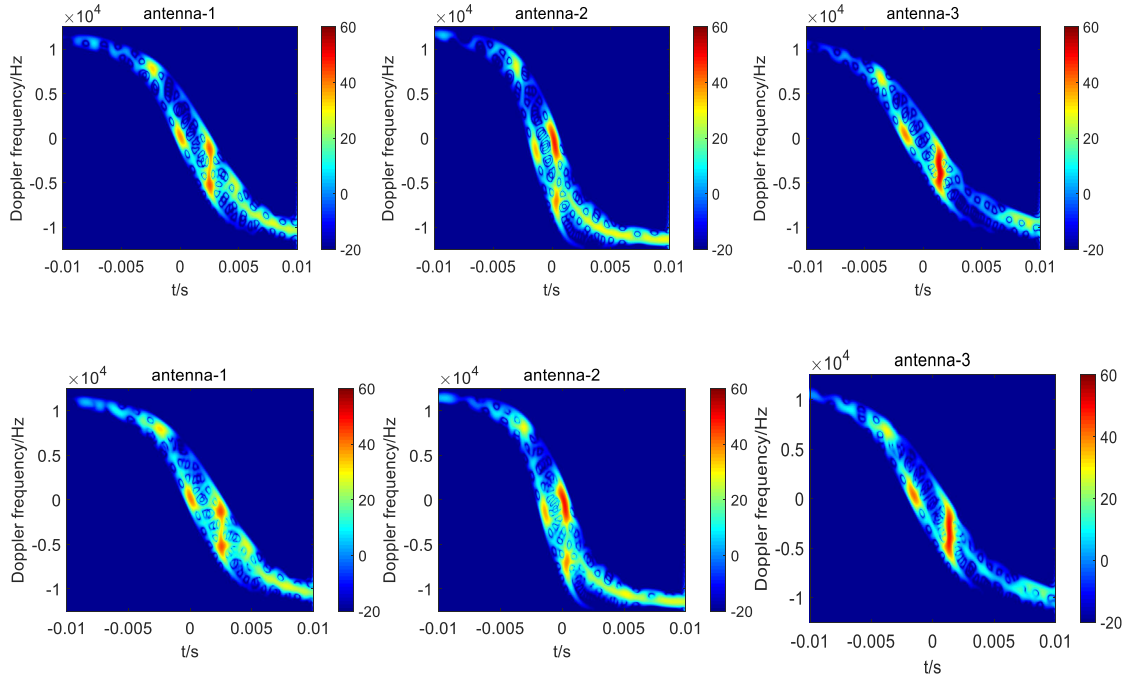
**Table C4** Parameters estimation results for Object-1 under SNR=15 dB and SNR=10 dB

Parameters (unit)	15 dB	Absolute Error	10 dB	Absolute Error
$X_{cpa}$ (m)	2.537	0.0208	2.6311	0.1149
$Y_{cpa}$ (m)	2.1935	0.2987	2.2377	0.3429
$Z_{cpa}$ (m)	-1.1397	0.1484	-1.1506	0.1593
$r$ (m)	3.4685	0.1685	3.5329	0.2329
$v$ (m/s)	602.8103	2.8103	604.8146	4.8146
$\alpha_v$ ( $^\circ$ )	-16.0611	0.8389	-15.2956	1.6044
$\beta_v$ ( $^\circ$ )	31.9829	3.8829	31.7198	3.6198
$\alpha_r$ ( $^\circ$ )	-23.1639	5.5361	-21.2244	7.4756
$\beta_r$ ( $^\circ$ )	28.4199	3.1801	27.6581	3.9419

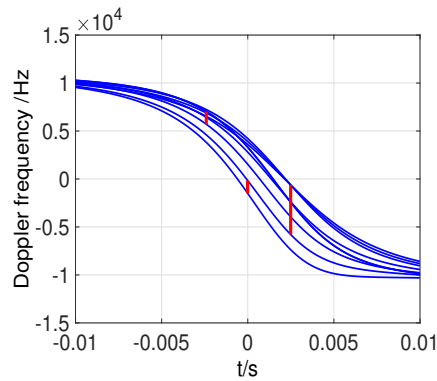
The estimated results for the case of three antennas under different level of SNR is showed in Table C4. The estimation results show the proposed method is robust in noisy condition. For the case of SNR=15 dB, the errors of the coordinates of CPA ( $X_{cpa}, Y_{cpa}, Z_{cpa}$ ) are less than 0.3 m; the error of scalar miss distance is less than 0.2 m; the error of scalar velocity is less than 3 m/s; and the errors of attitude angles are less than  $6^\circ$ .

The comparison between the TFRs of simulated results and that computed by the full-wave method is provided in Figure C1. With the estimated parameters, TFRs of three receiving antennas simulated by the models and those computed

by the full-wave method show good similarity of 0.922, 0.941 and 0.947 in Figure C1. For better understanding the TFR signatures, the Doppler frequencies of LSCs and DSCs (contained in radar echoes of antenna-1) of Object-1 generated from the estimated VMD are presented in Figure C2.



**Figure C1** TFRs of the flying Object-1 (Upper: PMLFMA, Lower: SC model)



**Figure C2** Doppler frequencies of LSCs and DSCs of Object-1

## Appendix C.2 Object-2

There are distinct DSCs on the flanks of Object-2, and irregular edges of the fuselage. The coordinates of receiving antennas are shown in Table Appendix C.2. The motion parameters of Object-2 are shown in Table Appendix C.2. We assume that Object-2 is maneuvering in the flight, and the acceleration direction is perpendicular to the velocity direction. Based on the given motion parameters, the range of the elevation angle ( $\theta$ ) is about  $110^\circ \sim 175^\circ$  and the range of the azimuth angle ( $\phi$ ) is about  $0^\circ \sim 160^\circ$  in the short time interval (about 0.02 s) when the object is approaching the CPA.

**Table C5** Antenna array coordinates

Number	$X_i$ (m)	$Y_i$ (m)	$Z_i$ (m)
1	0.5169	0	0.731
2	0.5169	0.731	0
3	0.5169	-0.731	0

**Table C6** Simulation parameters

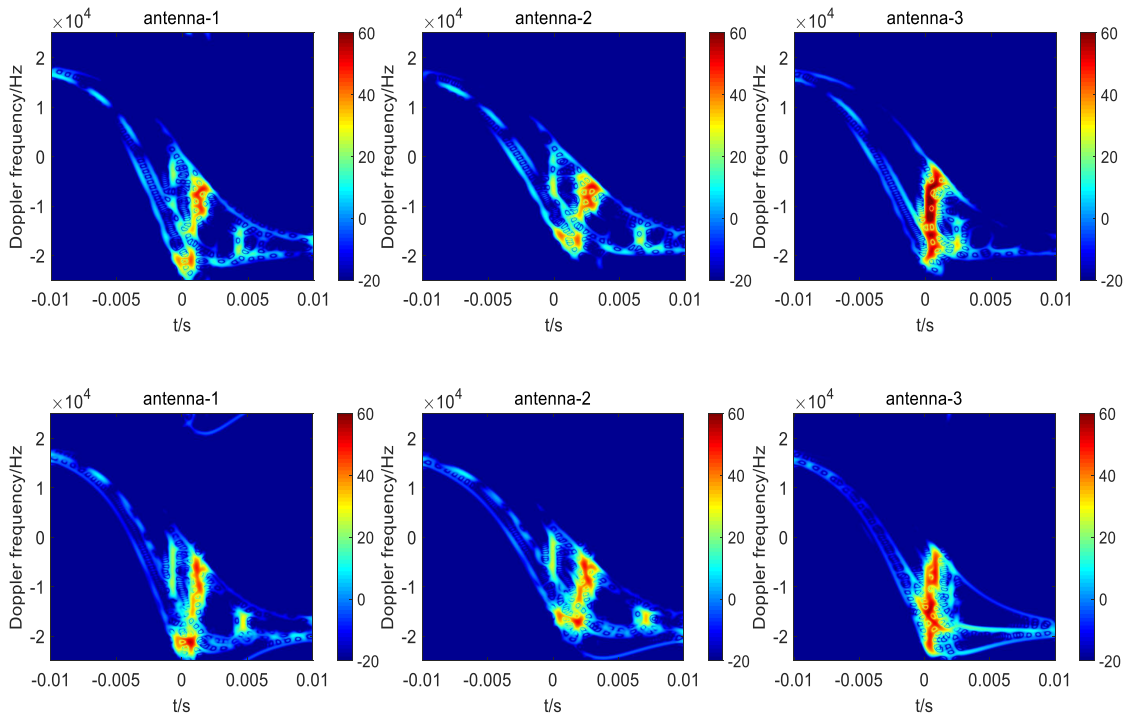
Parameters (unit)	Value	Parameters (unit)	Value
$X_{cpa}$ (m)	2.1505	$\alpha_v$ ( $^\circ$ )	30
$Y_{cpa}$ (m)	-1.5412	$\beta_v$ ( $^\circ$ )	110
$Z_{cpa}$ (m)	3	$\alpha_r$ ( $^\circ$ )	40
$r$ (m)	4	$\beta_r$ ( $^\circ$ )	110
$v$ (m/s)	600	$a$ (m/s <sup>2</sup> )	346

**Table C7** Parameters estimation results of Object-2

Parameters (unit)	Non-noise	Absolute Error	15 dB	Absolute Error	10 dB	Absolute Error
$X_{cpa}$ (m)	2.1925	0.042	2.4031	0.2526	2.4641	0.3136
$Y_{cpa}$ (m)	-1.5788	0.0376	-1.9839	0.4427	-2.1465	0.6053
$Z_{cpa}$ (m)	2.9041	0.0959	2.7255	0.2745	3.2183	0.2183
$r$ (m)	3.9665	0.0335	4.2037	0.2037	4.2121	0.2121
$v$ (m/s)	599.0875	0.9125	603.7934	3.7934	592.8679	7.1321
$\alpha_v$ ( $^\circ$ )	31.0021	1.0021	28.9627	1.0373	28.0819	1.9181
$\beta_v$ ( $^\circ$ )	110.1605	0.1605	113.7047	3.7047	119.1743	9.1743
$\alpha_r$ ( $^\circ$ )	40.2121	0.2121	39.4732	0.5268	45.7754	5.7754
$\beta_r$ ( $^\circ$ )	109.3925	0.6075	111.8658	1.8658	113.3944	3.3944

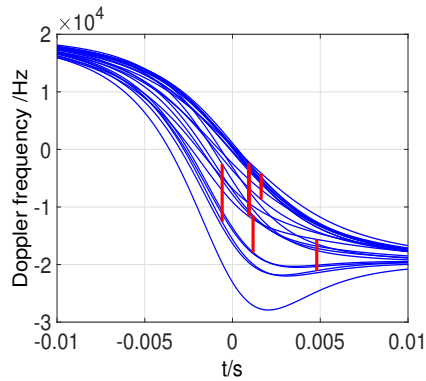
The estimated results without considering noise and the results under different level of SNR are showed in Table C7. For the case of SNR= 15 dB, the errors of coordinates of CPA (  $X_{cpa}$ ,  $Y_{cpa}$ ,  $Z_{cpa}$  ) are less than 0.5 m, the error of the scalar miss distance is less than 0.3 m ; the error of the scalar velocity is less than 4 m/s; and the errors of attitude angles are less than 4 $^\circ$ .

The comparison between the TFRs simulated by the SC models and those computed by the full-wave method are provided in Figure C3. With the estimated parameters, TFRs of three receiving antennas simulated by the models and those computed by the full-wave method show good similarity of 0.881, 0.887 and 0.891 in Figure C3. The Doppler frequencies of LSCs and DSCs (contained in radar echoes of antenna-1) of Object-2 generated from the estimated VMD are presented in Figure C4.



**Figure C3** TFRs of flying Object-2(Upper: PMLFMA, Lower: SC model)

Through a serial of numerical analysis, we found that the image signatures of the TFRs are much sensitive to the following parameters (in order of sensitivity):  $\beta_v$ ,  $\alpha_r$ ,  $\beta_r$ ,  $\alpha_v$ ,  $X_{cpa}$  and  $Y_{cpa}$  for the given motion setting of above cases. The TFR



**Figure C4** Doppler frequencies of LSCs and DSCs of Object-2

of Object-1 is more sensitive to  $X_{cpa}$  than  $Y_{cpa}$ , in contrast with Object-2.

From the estimated results, we can see that the accuracy of the SC modeling for Object-1 is higher than that of Object-2. However, the estimation errors of the VMD are worse than those of Object-2. That is due to the following reasons: the geometry structure of Object-2 is more complex than that of Object-1. It has more SSCs and DSCs which are sensitive to the change of aspect angles, which bring advantages for the attitude angles estimation, whereas, disadvantages for the SC modeling. Therefore, on the one hand, these SCs increase the errors of SC modeling. On the other hand, because of their aspect angle sensitivity, the estimation accuracy of attitude angles is high.

#### References

- 1 Ma L, Liu J, Wang T, et al. Micro-Doppler characteristics of sliding-type scattering center on rotationally symmetric target. *Science China(Information Sciences)*, 2011, 54(9): 1957-1967.
- 2 Guo K Y, Xiao G L, Zhai Y, et al. Angular glint error simulation using attributed scattering center models. *IEEE Access*, 2018, 6: 35194-35205.
- 3 Pan X M, Sheng X Q. A sophisticated parallel MLFMA for scattering by extremely large targets. *IEEE Antennas and Propagation Magazine*, Jun 2008, 50: 129-138.
- 4 Auger F, Flandrin P. Improving the readability of time-frequency and time-scale representations by the reassignment method. *IEEE Transactions on Signal Processing*, May 1995, 43: 1068-1089.